AMERICAN SOCIETY FOR MICROBIOLOGY | mBio®

RESEARCH ARTICLE

Identification and Characterization of a Phase-Variable Element That Regulates the Autotransporter UpaE in Uropathogenic *Escherichia coli*

E. J. Battaglioli,[a,b] K. G. K. Goh,[c] T. S. Atruktsang,[a] K. Schwartz,[a] M. A. Schembri,[c] R. A. Welch[a]

[a]Department of Medical Microbiology and Immunology, School of Medicine and Public Health, University of Wisconsin—Madison, Madison, Wisconsin, USA

[b]Department of Medicine, Division of Gastroenterology and Hepatology, Mayo Clinic, Rochester, Minnesota, USA

[c]School of Chemistry and Molecular Biosciences, University of Queensland, Brisbane, QLD, Australia

ABSTRACT Uropathogenic *Escherichia coli* (UPEC) is the most common etiologic agent of uncomplicated urinary tract infection (UTI). An important mechanism of gene regulation in UPEC is phase variation that involves inversion of a promoter-containing DNA element via enzymatic activity of tyrosine recombinases, resulting in biphasic, ON or OFF expression of target genes. The UPEC reference strain CFT073 has five tyrosine site-specific recombinases that function at two previously characterized promoter inversion systems, *fimS* and *hyxS*. Three of the five recombinases are located proximally to their cognate target elements, which is typical of promoter inversion systems. The genes for the other two recombinases, IpuA and IpuB, are located distal from these sites. Here, we identified and characterized a third phase-variable invertible element in CFT073, *ipuS*, located proximal to *ipuA* and *ipuB*. The inversion of *ipuS* is catalyzed by four of the five CFT073 recombinases. Orientation of the element drives transcription of a two-gene operon containing *ipuR*, a predicted LuxR-type regulator, and *upaE*, a predicted autotransporter. We show that the predicted autotransporter UpaE is surface located and facilitates biofilm formation as well as adhesion to extracellular matrix proteins in a K-12 recombinant background. Consistent with this phenotype, the *ipuS* ON condition in CFT073 results in defective swimming motility, increased adherence to human kidney epithelial cells, and a positive competitive kidney colonization advantage in experimental mouse UTIs. Overall, the identification of a third phase switch in UPEC that is regulated by a shared set of recombinases describes a complex phase-variable virulence network in UPEC.

IMPORTANCE Uropathogenic *Escherichia coli* (UPEC) is the most common cause of urinary tract infection (UTI). ON versus OFF phase switching by inversion of small DNA elements at two chromosome sites in UPEC regulates the expression of important virulence factors, including the type 1 fimbria adhesion organelle. In this report, we describe a third invertible element, *ipuS*, in the UPEC reference strain CFT073. The inversion of *ipuS* controls the phase-variable expression of *upaE*, an autotransporter gene that encodes a surface protein involved in adherence to extracellular matrix proteins and colonization of the kidneys in a murine model of UTI.

KEYWORDS autotransporter proteins, phase switch, tyrosine recombinases, urinary tract infection, uropathogenic *E. coli*

Urinary tract infections (UTIs) are one of the most common infections diagnosed in clinics and hospitals. Nearly 50% of women will experience a UTI in their lifetime with treatment costs exceeding $3.5 billion annually in the United States (1, 2). The most common etiologic agent of uncomplicated UTIs is uropathogenic *Escherichia coli*

Received 26 June 2018 **Accepted** 28 June 2018 **Published** 7 August 2018

Citation Battaglioli EJ, Goh KGK, Atruktsang TS, Schwartz K, Schembri MA, Welch RA. 2018. Identification and characterization of a phase-variable element that regulates the autotransporter UpaE in uropathogenic *Escherichia coli*. mBio 9:e01360-18. https://doi.org/10.1128/mBio.01360-18.

Editor Gary M. Dunny, University of Minnesota Medical School

Address correspondence to R. A. Welch, rawelch@wisc.edu.

This article is a direct contribution from a Fellow of the American Academy of Microbiology. Solicited external reviewers: Harry Mobley, University of Michigan; Matthew Mulvey, University of Utah School of Medicine.

(UPEC), which accounts for ~80% of reported infections (3). The predicted reservoir of UPEC is the colon, and infection follows an ascending route, which is initiated via colonization of the urethra. Bacteria that gain access to the urinary tract face a variety of host defense mechanisms, including shedding of uroepithelial cells, low iron levels, rapid recruitment of phagocytes, host-derived antimicrobial peptides, and the cleansing flow of urine (4–11). Additionally, recent characterization of a urinary tract-specific microbiome suggests that there may also be microbial barriers to infection as is observed in the gut (12, 13). To establish and maintain an infection, UPEC possesses specialized virulence factors to overcome these defense mechanisms. Well-described examples include adhesive fimbriae, multiple iron acquisition systems, a polysaccharide capsule, effective reactive nitrogen species detoxification systems, and toxins such as hemolysin (14–21).

Type 1 fimbriae are polytrichous hairlike projections expressed on the surface of UPEC cells (22). They mediate attachment and invasion of the bladder epithelium, are a key component of the "stick-or-swim" lifestyle choice, and are critical to the establishment and maintenance of infection in the murine model of UTI (14, 15, 23, 24). Type 1 fimbriae were also recently shown to facilitate adherence to colonic epithelial cells and persistence in the gut (25). The expression of type 1 fimbriae is phase variable as a result of rearrangement of the invertible element or "switch" *fimS*, which contains a promoter (26, 27). In *E. coli* K-12, inversion of *fimS* is catalyzed by the proximally carried genes for the tyrosine site-specific recombinases FimB and FimE (28). In addition to the recombinases, multiple DNA binding proteins, including integration host factor (IHF), leucine responsive protein (LRP), and histone-like nucleoid structuring (H-NS), interact with *fimS* to facilitate formation of the appropriate DNA conformation necessary for Holliday junction formation and recombination (29–33). Associated changes in expression and activity of both the recombinases and the accessory DNA binding proteins alter switching kinetics and result in population-wide changes of phase state (34–37). Additionally, cross talk with genes from other adhesive fimbriae and specific environmental conditions, including pH, osmolarity, temperature, and metabolite availability, are known to facilitate these population phase-state biases (38–43). In total, these regulatory mechanisms are predicted to adapt a population phase to suit changing metabolic and environmental cues.

In addition to these methods of regulation, CFT073 has three additional tyrosine recombinases, FimX, IpuA, and IpuB, which are conserved in many UPEC strains (23). FimX and IpuA are also capable of catalyzing inversion of *fimS* in CFT073 despite being located distal to *fimS* on the CFT073 chromosome (23). Typically, site-specific recombinases that mediate inversion of phase switches are encoded proximal to their sites of functionality, suggesting the existence of other switches local to the three UPEC-specific recombinases (44). Recently, a second phase-variable element, *hyxS*, was characterized proximal to *fimX* in CFT073 and another UPEC strain, UTI89 (45). Inversion of *hyxS* regulates expression of *hyxR*, a LuxR-type regulator. Only FimX is capable of catalyzing inversion of this switch, and *hyxS*-dependent expression of *hyxR* affects resistance to reactive nitrogen species and intracellular macrophage survival, although the precise mechanisms underlying these effects remain to be characterized (45). Phase-variable switching at *fimS* and *hyxS* has also been examined in UPEC strains from the globally disseminated multidrug-resistant ST131 clone, which possesses functional FimE and FimX recombinases (46).

Because there are known invertible DNA elements proximal to *fimB*, *fimE*, and *fimX*, we sought to determine if a third phase switch existed proximal to *ipuA* and *ipuB*. Here, we report the identification of a third phase-variable switch in CFT073, *ipuS*, located adjacent to the *ipuA* and *ipuB* recombinase genes. The switch is bounded by a set of 7-bp inverted repeats, and the recombination half-sites share sequence similarity with the *fimS* and *hyxS* invertible elements. Transcriptional analysis identifies the presence of the transcription start site in the element, and four of the five recombinases (FimB excluded) are able to independently catalyze *ipuS* inversion. Inversion of the element affects transcription of *ipuR*, a predicted LuxR-type regulator and *upaE*, a predicted

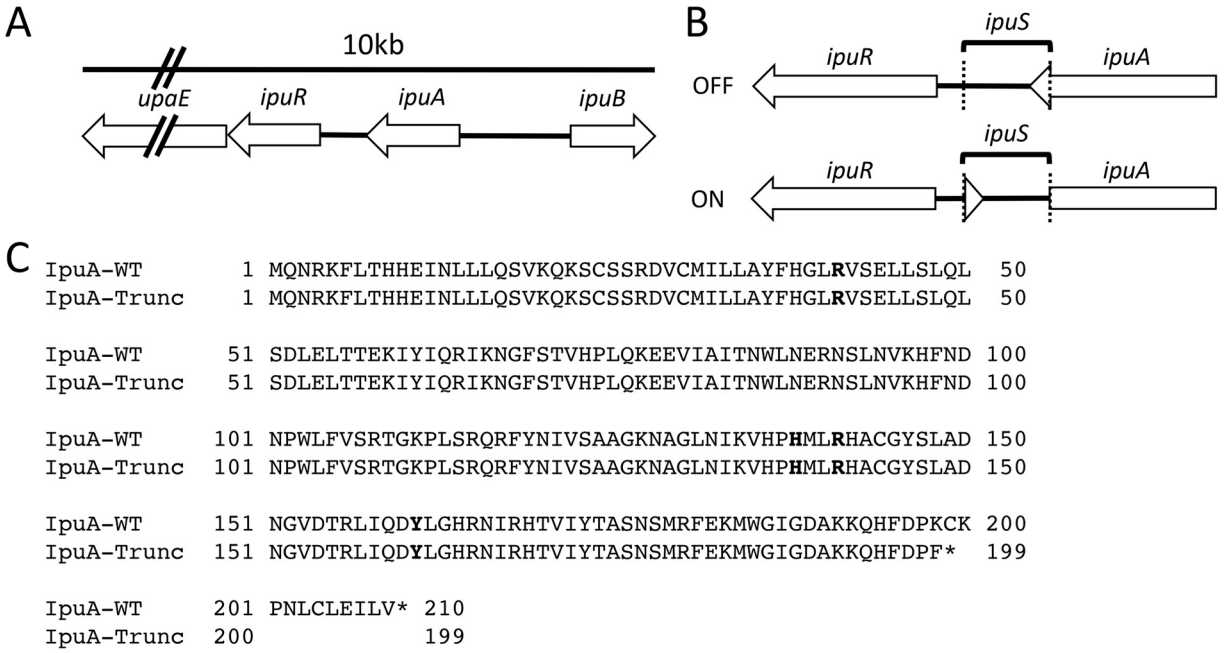

FIG 1 Identification of the *ipuS* invertible element. (A) Schematic representation of the genomic context of *ipuS*. (B) DNA rearrangement as a result of *ipuS* inversion. The ON/OFF state is defined by expression of a *lacZ-ipuR* transcriptional fusion in the pictured orientation. The location of the inverted repeats is indicated by the dotted lines. (C) Inversion to the ON state results in an 11-amino-acid truncation of *ipuA* and a K-to-F replacement of the truncated form's terminal amino acid. Conserved RHRY active-site residues are indicated in bold and unaffected by the truncation.

autotransporter. Phenotypic characterization of UpaE reveals that it is exposed at the cell surface and can facilitate biofilm formation as well as adhesion to human extracellular matrix (ECM) proteins. Further analysis of *ipuS* inversion reveals that a locked-ON state results in a defect in swimming motility, increased adherence to kidney epithelial cells, and a 5-fold advantage in colonization of the kidneys at 72 h postinfection (hpi). Overall, this work identifies a UPEC switch that controls the phase-variable expression of UpaE, an autotransporter that may contribute to UPEC infection in the complex, diverse microenvironments of the urinary tract.

RESULTS

Identification of a phase-variable element, *ipuS*. Previous studies identified inversion sites associated with the FimB, FimE, and FimX tyrosine recombinases in CFT073 (23, 45). In most other characterized tyrosine recombinase-mediated phase variation systems, the recombinases are active on closely linked invertible DNA elements. Thus, we hypothesized that there would be an invertible element proximal to the *ipuA* and *ipuB* recombinase genes. Immediately 5′ of *ipuA* is a putative two-gene operon containing *ipuR* (encoding a predicted LuxR-type regulator) and *upaE* (encoding a predicted autotransporter protein). Further analysis of this DNA region reveals that *ipuA* and *ipuR* are separated by a 317-bp intergenic spacer with no predicted open reading frames (Fig. 1A). The size of the spacer is consistent with other promoter inversion systems, suggesting that it may contain an invertible element. To test this, a chromosomal *ipuR-lacZ* transcriptional fusion was generated (strain WAM5009) to detect inversion events in this region. When a stationary-phase LB broth culture of WAM5009 was plated on MacConkey's lactose medium, the reporter strain displayed a mixture of red and white colonies. The region containing the predicted invertible element was amplified by PCR from a red and a white colony, respectively, and sequenced by Sanger dideoxy chain termination. The DNA sequences from the two colony types revealed the presence of a 260-bp invertible element, which we refer to as *ipuS* (Fig. 1B). The *ipuS* element is bounded by a pair of 7-bp inverted repeats with

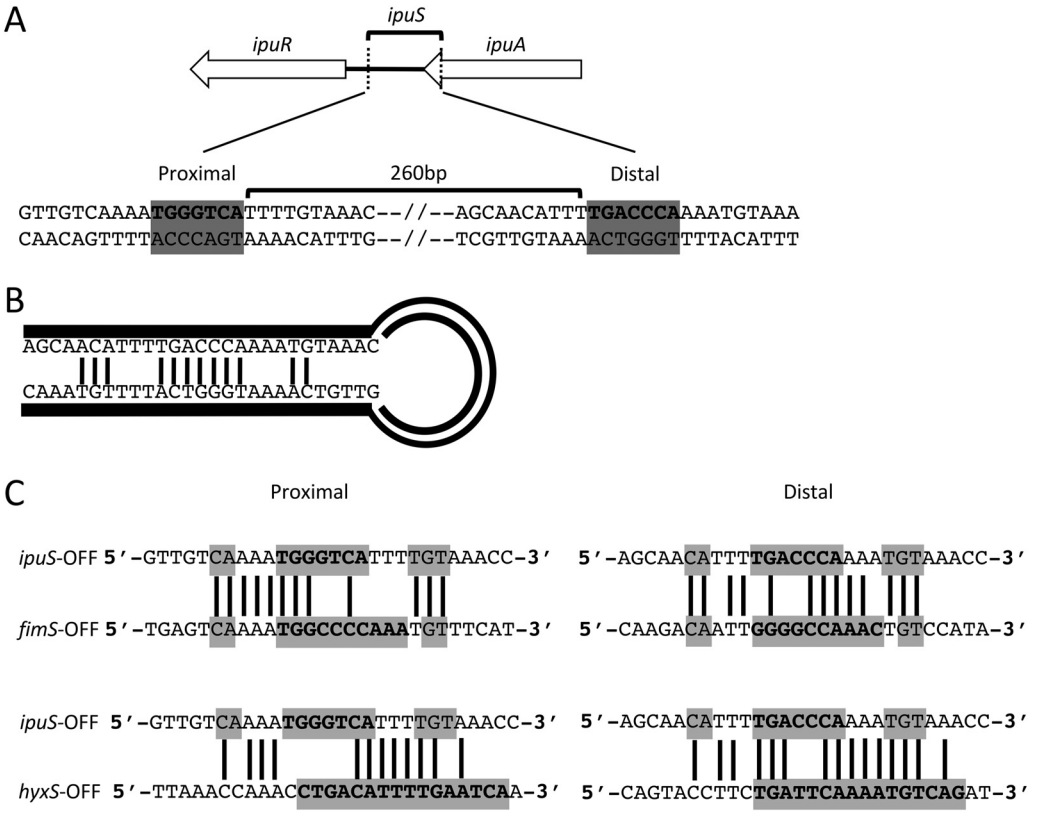

FIG 2 *ipuS* invertible element characterization. (A) The invertible element is 260 bp and is defined by a pair of 7-bp inverted repeats shown in bold with a gray background. (B) DNA hairpin created during recombination. Putative base pair interactions between the core inverted repeat and local flanking sequence are indicated by connecting lines. (C) Comparison of *ipuS* versus *fimS* inverted repeat sequences (top panel) and *ipuS* versus *hyxS* inverted repeat sequences (bottom panel). Proximal and distal half-sites are shown on the left and right, respectively. Inverted repeat sequence and surrounding sequences that can participate in base pairing during recombination are boxed in gray, and sequence identity is indicated by connecting bars. Nucleotides that are components of the core inverted repeats for each switch are shown in bold.

the distal inverted repeat located within the annotated coding sequence of *ipuA* (Fig. 1B). In the OFF state, defined as lack of expression from the *ipuR-lacZ* transcriptional fusion, the full-length form of IpuA is produced. Upon inversion to the ON state, defined as expression of the *ipuR-lacZ* fusion, a truncation of the *ipuA* coding sequence occurs. The truncation removes 11 amino acids from the C terminus of IpuA and generates a K-L substitution of the terminal amino acid (Fig. 1C). None of the four required RHRY active-site residues for IpuA are altered by the truncation, suggesting that the shortened form may retain catalytic activity (Fig. 1C).

***ipuS* half-site analysis.** The *ipuS* invertible element is defined by a pair of 7-bp inverted repeats (Fig. 2A). *ipuS* has the shortest inverted repeats of the three described elements in CFT073, with *fimS* and *hyxS* having 9- and 16-bp repeats, respectively (27, 45). In addition to the core repeat sequence, up to 5 bp surrounding the core can participate in base pairing and help facilitate inversion. The sequence of these residues is similar to the respective required regions of *fimS* (22), and the predicted hairpin structure generated during recombination illustrates these potential base-pairing interactions (Fig. 2B).

The inverted repeats and surrounding sequence of *ipuS* were compared to the same respective regions of *hyxS* and *fimS* to assess the potential of shared recombinase activity among the elements. For consistency, the OFF state of each element was used for the comparisons. The *ipuS* switch shares a high degree of sequence similarity with the other two switches, particularly *fimS* (Fig. 2C). In this figure, lines connecting bases indicate sequence identity, the inverted repeat sequence is shown in bold, and the gray

TABLE 1 Strains and plasmids used in this study

Strain, plasmid, or cell line	Description	Reference or source
Bacterial strains		
WAM2266	CFT073 Nal; urosepsis isolate	18
WAM5009	CFT073 with pFUSE *ipuR* txn fusion	This study
WAM5063	CFT073 Nal *fimBE fimX ipuA ipuB* (*fimS* OFF, *ipuS* OFF)	This study
WAM5064	CFT073 Nal *fimBE fimX ipuA ipuB* (*fimS* ON, *ipuS* ON)	This study
WAM5065	CFT073 Nal *fimBE fimX ipuA ipuB* (*fimS* ON, *ipuS* OFF)	This study
WAM5088	CFT073 Nal *fimBE fimX ipuA ipuB* (*fimS* OFF, *ipuS* ON)	This study
WAM5144	WAM5063 *lacZYA*	This study
WAM5145	WAM5064 *lacZYA*	This study
WAM5146	WAM5065 *lacZYA*	This study
WAM5147	WAM5088 *lacZYA*	This study
WAM5070	WAM5064 with pACYC184	This study
WAM5079	WAM5064 with pACYC177	This study
WAM5071	WAM5064 with pWAM2801	This study
WAM5081	WAM5064 with pWAM2957	This study
WAM5072	WAM5064 with pWAM2961	This study
WAM5080	WAM5064 with pWAM2775	This study
WAM5082	WAM5064 with pWAM3579	This study
WAM5073	WAM5064 with pWAM5073	This study
WAM5074	WAM5065 with pACYC184	This study
WAM5083	WAM5065 with pACYC177	This study
WAM5075	WAM5065 with pWAM2801	This study
WAM5085	WAM5065 with pWAM2957	This study
WAM5076	WAM5065 with pWAM2961	This study
WAM5084	WAM5065 with pWAM2775	This study
WAM5077	WAM5065 with pWAM3759	This study
WAM5078	WAM5065 with pWAM5073	This study
MS427	*E. coli* expression strain	48
MS427(pUpaE)	MS427 with pSU2718::*upaE*	This study
Plasmids		
pKD46	Lambda Red recombinase helper plasmid	92
pCP20	FLP helper plasmid	92
pKD4	*kan*$^+$ template	92
p2779	pFUSE *lacZYA* transcriptional fusion suicide vector	93
pACYC177	Cloning plasmid with constitutively active promoter	New England BioLabs
pACYC184	Cloning plasmid with expression driven by the insert promoter	New England BioLabs
pMal-p2x	Cloning plasmid for MBP-assisted protein purification	New England BioLabs
pSU2718	Low-copy-number cloning plasmid for exogenous expression in *E. coli*	46
pWAM2801	pACYC177 *fimB*; Kan^r	23
pWAM2957	pACYC177 *fimE*; Kan^r	23
pWAM2775	pACYC177 *ipuB*; Kan^r	23
pWAM2961	pACYC177 *ipuA-FL*; Kan^r	23
pWAM3579	pACYC184 *ipuA-FL*; Cm^r	23
pWAM5073	pACYC184 *ipuA-Trunc*; Cm^r	This study
pUpaE	pSU2718 *upaE*	This study
Cell line A-498	Human kidney epithelial carcinoma cells	ATCC

boxes indicate potential base-pairing interactions. Previous reports comparing the half-sites of *hyxS* and *fimS* show only limited similarity (45).

Recombinase activity at *ipuS*. The activity of tyrosine recombinases at *fimS* and *hyxS* is known to be sequence specific, and the similarity between the *ipuS*, *fimS*, and *hyxS* inverted repeats suggests that many, if not all, of the five recombinases would have activity at *ipuS*. To test this, the five recombinases were deleted by sequential Lambda Red mutagenesis and ϕEB49 phage transduction to lock the orientation of all three switches. In the case of *ipuA*, a 404-bp truncation from the 5′ end was generated to remove one of the required active-site residues, rendering the resulting protein nonfunctional while preserving the *ipuS* distal inverted repeat and allowing for inversion via exogenous expression of the recombinases. Strains were created with all four possible combinations of *ipuS* and *fimS* phase states. *hyxS* was locked OFF in all strains examined (Table 1).

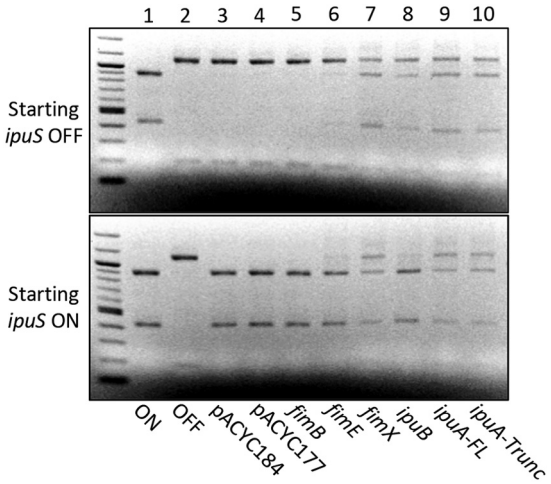

FIG 3 Assessment of each recombinase's ability to catalyze inversion of *ipuS in vitro*. Ethidium bromide-stained electrophoretic gels of PacI-digested PCR products are shown. Lanes 1 and 2 contain digested PCR products from CFT073 *ipuS* phase locked-ON (WAM5064) and -OFF (WAM5065) strains generated by 5-way recombinase deletion. Lanes 3 and 4 contain digested PCR products from vector-only controls (WAM5070, WAM5079, WAM5074, and WAM5083). Lanes 5 to 10 contain PCR products from the locked-OFF strain WAM5065 (top panel) or locked-ON strain WAM5064 (bottom panel) after transforming each with a recombinant plasmid containing the indicated recombinase. Both the full-length and truncated forms of *ipuA* were tested for activity (lanes 9 and 10).

Each recombinase, including the full-length (FL) and truncated (Trunc) forms of IpuA, was provided in *trans* on multicopy expression constructs in both the *ipuS* ON- and OFF-locked backgrounds. All the recombinase complementation plasmids were constructed in a pACYC177 background and constitutively expressed, except for IpuA-FL and IpuA-Trunc. These were constructed in a pACYC184 background with the native *ipuA* promoter driving expression. In a previous publication, we showed that expression of *ipuA* under the control of the kanamycin resistance gene promoter on pACYC177 causes cell morphology defects and that expression from its native promoter rectifies this complication (23).

The ability of a single recombinase to switch the orientation from a starting ON or OFF state at *ipuS* was assayed by PCR amplification of the switch and asymmetrical restriction digestion of the resulting product by PacI. With the exception of FimB, all the recombinases are independently capable of catalyzing inversion in both directions, including the truncated form of IpuA (Fig. 3). FimB showed no detectable catalytic activity under the conditions tested. However, the same pACYC177::*fimB* construct was capable of inverting *fimS*, demonstrating that the lack of activity is not due to complications with recombinant plasmid expression (23). The inversion assay is not explicitly quantitative; however, inspection of the intensity of the bands in the digest suggests that there may be differences in catalytic efficiency among the recombinases. FimE is less efficient than IpuA-FL, IpuA-Trunc, IpuB, and FimX at inverting the *ipuS* switch in both directions under the conditions tested (Fig. 3). IpuB also displays a reduced capacity to catalyze ON-to-OFF inversion (Fig. 3).

Identification of a putative promoter in *ipuS*. We postulated that the invertible element could regulate transcription of *ipuR-upaE* by containing an additional promoter or by blocking readthrough of an upstream *ipuA*-associated promoter. To test this, we subjected the *ipuS* region to 5′ rapid amplification of cDNA ends (RACE) using cDNA generated from *ipuS* phase-locked-ON and -OFF strains. Only the locked-ON strain generated a product, and subsequent sequencing revealed the location of a putative transcriptional start site in *ipuS* (Fig. 4A). Sequence analysis immediately upstream of the mapped transcriptional start site revealed a putative promoter with −35 and −10 sequences that each have 4 of 6 nucleotides matching the sigma-70 consensus sequence (Fig. 4B) (47).

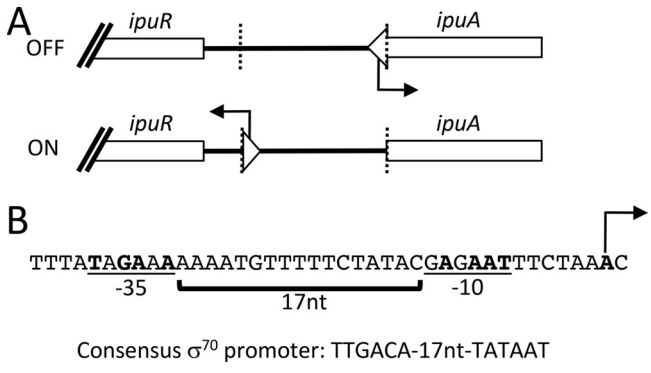

FIG 4 *ipuS* promoter mapping by 5′ RACE. (A) The *ipuS* transcription start site was identified by 5′ RACE and is located within the full-length *ipuA* coding sequence. Inversion of element to the "ON" state orientates the promoter toward *ipuR/upaE*. The inverted repeats are indicated by the dotted lines. (B) A predicted promoter was identified in proximity to the mapped transcription start site that most closely matches a σ^{70} consensus promoter. Locations of the predicted −35 and −10 regions, spacer lengths, and transcription start site are indicated. Bases matching consensus are shown in bold.

UpaE is localized to the cell surface. We next sought to characterize phenotypic effects of the *ipuS* ON versus OFF phase state and began by assessing the functionality of the regulated genes *upaE* and *ipuR*. Initial genetic studies examining the role of *ipuR* did not reveal any clear phenotype, so we focused on characterization of the predicted autotransporter gene *upaE*. To assess the functionality of UpaE in isolation, we utilized a plasmid-based overexpression system in the *E. coli* K-12 background strain MS427 (48). MS427 has a mutation in the Ag43-encoding *flu* gene, rendering it unable to facilitate biofilm formation or self-aggregation, and has previously been used successfully to probe the function of other autotransporters (20, 48–53). Immunoblot assays of whole-cell lysates generated from MS427 transformed with a UpaE expression plasmid using a polyclonal antiserum raised to a UpaE-maltose binding protein (MBP) fusion protein showed a band consistent with the 271-kDa predicted molecular weight of UpaE (Fig. 5A). UpaE localization was then assessed using immunofluorescence microscopy, which showed staining concentrated to the cell membrane, suggesting that it is membrane bound (Fig. 5B). Further assessment in the native CFT073 context yielded similar results. We probed for the expression of UpaE in whole-cell lysates and culture supernatants of the phase-locked-ON and -OFF CFT073 strains. UpaE was detectable only in phase-locked-ON cells (Fig. 5C). Additionally, extracellular UpaE species were not detected in concentrated 10-ml trichloroacetic acid (TCA) preparations from culture supernatants of either locked-ON or locked-OFF strains (Fig. 5C). This further corroborates the immunofluorescence data in the MS427 background and suggests that UpaE is membrane associated in the native CFT073 context (Fig. 5C).

UpaE mediates biofilm formation and adhesion to ECM proteins. After assessing expression and localization, we probed the functionality of UpaE. As surface-bound autotransporters are frequently involved in biofilm formation or adherence, we assessed biofilm production. The parent strain MS427 is unable to form biofilms, but introduction of the plasmid-borne copy of UpaE resulted in a significant increase in biofilm production when assessed by crystal violet staining (Fig. 6A). We also investigated the ability of UpaE to mediate adherence to human extracellular matrix (ECM) proteins. Adherence to MaxGel, a commercially available mixture of collagens, laminin, fibronectin, tenascin, elastin, and a number of proteoglycans and glycosaminoglycans, was significantly increased in the UpaE overexpression strain compared to empty vector controls (Fig. 6B). Further examination revealed that UpaE mediates significant adherence to fibronectin, laminin, and collagens I, II, and V specifically (Fig. 6B). Together, these results suggest that UpaE is a surface-exposed autotransporter and facilitates both biofilm formation and adherence to human ECM proteins.

Phenotypes of the *ipuS* ON versus OFF phase states in CFT073. Due to the conservation of this region in many UPEC strains and the known links between

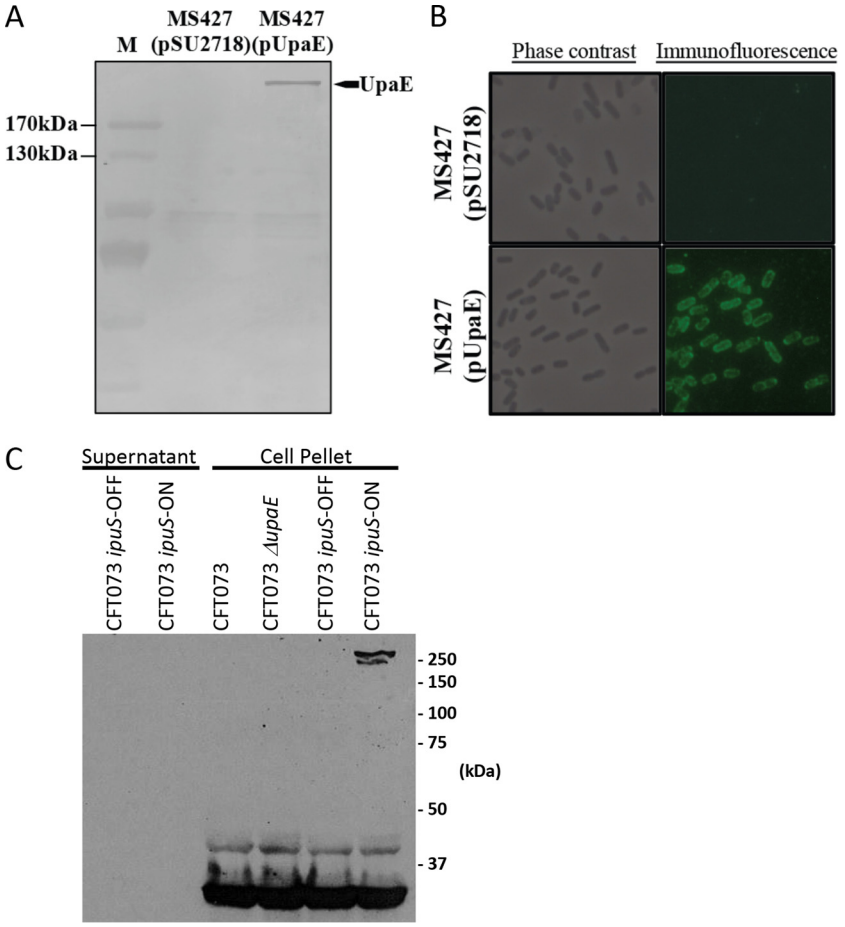

FIG 5 Expression and surface localization of UpaE in *E. coli* K-12. (A) Western blot analysis of whole-cell lysates prepared from MS427(pSU2718) vector control and MS427(pUpaE). A band corresponding to UpaE (271 kDa) was detected in MS427(pUpaE) but not in the MS427(pSU2718) control. Lane M refers to molecular weight markers; the 170-kDa and 130-kDa proteins are indicated. (B) Phase-contrast and immunofluorescence microscopy using specific antisera against UpaE. Positive reactions indicating the surface localization of UpaE were detected in MS427(UpaE) (bottom) but not in the MS427(pSU2718) vector control (top). (C) Western blot analysis of pelleted cells solubilized in crack buffer or concentrated 10-ml TCA precipitations of culture supernatants. Protein detection was performed using a polyclonal antiserum raised to an UpaE-MBP fusion protein. A band consistent with the predicted 271-kDa size of UpaE is present only in the cellular fraction of phase locked-ON cells.

adherence-promoting autotransporters and phase variation in pathogenesis (20, 21, 54–58), we predicted that inversion would play a role in virulence-related phenotypes. We previously demonstrated that in the *fimS* ON state there is a reduction in motility compared to the OFF position (23). Overnight liquid cultures were used to inoculate the surface of Adler's motility medium agar plates, and diameters of the swimming zones were measured after ~21 h of growth at room temperature. We observed that the *ipuS* OFF state is more motile than the *ipuS* ON state in a type 1 pilus OFF background (Fig. 7A). The same trend was observed in the type 1 pilus ON background; however, the nonmotile nature of type 1 pilus ON cells made it difficult to clearly discern the *ipuS* effects (Fig. 7A).

***ipuS* orientation affects colonization of the kidneys in a murine model of UTI and adherence to human kidney epithelial cells.** We next assessed if the *ipuS* phase state results in a difference in colonization in the murine model of UTI. To test this, we performed competition assays using the *ipuS* locked-ON and -OFF strains to address putative UpaE-dependent effects on colonization. A Δ*lacZYA* mutant variant of the *ipuS* locked-OFF strain (WAM5146) was used to facilitate generation of competitive indexes using MacConkey lactose medium. Previous experiments indicated that a Δ*lacZYA*

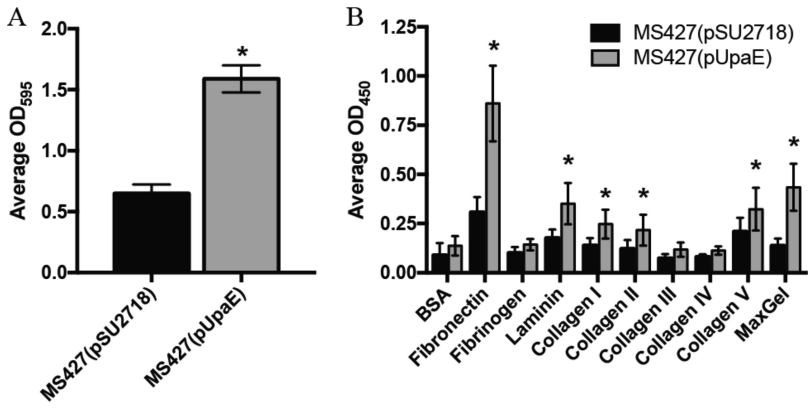

FIG 6 UpaE mediates biofilm formation and adhesion to ECM proteins. (A) Polystyrene 96-well microtiter plates (Corning) were used to monitor biofilm formation. Overnight cultures were subcultured 1/100 into fresh M9 minimal medium supplemented with 1 mM IPTG and incubated with shaking at 37°C for 24 h. Biofilms were stained with a 0.1% crystal violet solution and quantified by dissolving the crystal violet with an acetone-ethanol mix and measuring the OD_{595}. MS427(pUpaE) was able to form a better biofilm than the vector control. Experiments were performed in triplicate. *, $P < 0.05$, unpaired Student's *t* test. (B) MS427(pSU2718) vector control and MS427(pUpaE) were incubated in microtiter plates coated with ECM proteins. Nonadherent bacteria were washed off, and remaining bound cells were detected with a specific *E. coli* antiserum. MS427 overexpressing UpaE bound to fibronectin; laminin; collagens I, II, and V; and MaxGel. Experiments were performed in triplicate. *, $P < 0.05$, unpaired Student's *t* test.

mutant of CFT073 competes equally against wild-type (WT) CFT073 (59). Fifty-microliter inocula containing an equal ratio of the *ipuS* locked-ON and -OFF strains (totaling 10^8 CFU) were transurethrally delivered into the bladder of 6-week-old female CBA/J mice, and the infections were allowed to progress for 72 h. The animals were sacrificed, and their bladders and kidneys were excised, homogenized, and plated on MacConkey's lactose medium. Ratios of ON to OFF bacteria at sacrifice were normalized to the input ratio to generate relative competitive indexes (RCI). The type 1 fimbria locked-ON variants of the *ipuS* ON/OFF strains were used in the experiment because type 1 fimbria deletion strains are severely attenuated in mouse models of UTI (15). At 72 h postinfection (hpi), a 5-fold advantage ($P < 0.05$) for the *ipuS* ON state was observed in the kidneys (Fig. 7B). No difference was seen in the bladder at 72 hpi (Fig. 7B). To further assess the role of UpaE in facilitating infection *in vivo*, we also performed competition assays between WT CFT073 and an otherwise isogenic *ipuR/upaE* mutant. However, in this context no significant competitive difference was observed in the bladder or kidneys (see Fig. S1 in the supplemental material). We postulate that this is due to the phase-permissive background of the *ipuR/upaE* mutant strain. Locking *fimS* ON to help facilitate competitive infections in the *ipuS* ON/OFF strains also suppresses the production of P pilus (41), a kidney-specific adhesion factor. We predict that the ability of the *ipuR/upaE* mutant to produce P pili compensates for the difference observed between the *ipuS* OFF and ON strains.

The locked strains that were used in the competitive infection assays were virtually nonmotile due to the constitutive expression of type 1 pili (23). Importantly, this suggested that the *in vitro* swimming motility defect of WAM5088 was not the cause of the *ipuS*-dependent kidney colonization advantage. Rather, we speculated that the change in colonization was at least partially attributed to UpaE expression and its effect on adherence. To determine if the adhesive properties of UpaE may have contributed to the kidney-specific advantage observed *in vivo*, we assayed the four *ipuS/fimS* phase-locked strains for their ability to adhere to human kidney epithelial cells. The strains were incubated with confluent monolayers of A-498 cells (multiplicity of infection [MOI] of 10) for 1 h, and adherence was assessed by direct determination of CFU. The number of adherent bacteria was normalized to the input and expressed as percent adherence. Locking *ipuS* ON in a *fimS* OFF background increased adherence to kidney epithelial cells ($P < 0.05$), suggesting that expression of UpaE facilitates adhesion to the

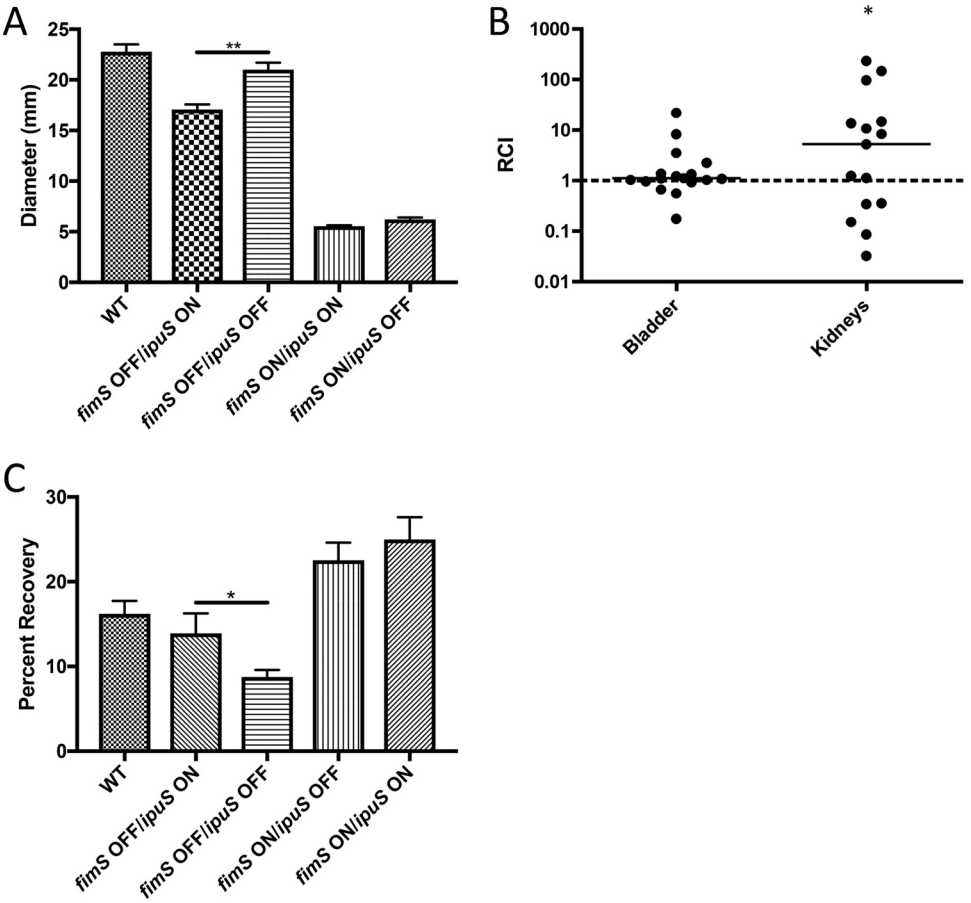

FIG 7 Phenotypic readouts of the *ipuS* phase state in a CFT073 background. (A) Swimming motility of phase-locked strains. One microliter of liquid culture normalized to an OD_{600} of 0.01 of each of the strains WAM2266 (WT), WAM5088 (*ipuS* ON/*fimS* OFF), WAM5063 (*ipuS* OFF/*fimS* OFF), WAM5064 (*ipuS* ON/*fimS* ON), and WAM5065 (*ipuS* OFF/*fimS* ON) was inoculated in the center of 7 plates containing Adler's motility medium. Values represent diameter of the swimming zone after ~21 h of room-temperature incubation (Mann-Whitney test, $P < 0.005$). (B) Seventy-two-hour competitive infection of WAM5064 (*fimS* ON, *ipuS* ON) versus WAM5146 (*fimS* ON, *ipuS* OFF, *lacZYA*). Relative competitive indexes were calculated from bladder and kidney homogenates at 72 hpi with lines representing the medians. WAM5064 (*ipuS* ON) has a 5-fold advantage in the kidneys (*, $P < 0.05$, Wilcoxon signed-rank test) at 72 hpi. (C) Adherence to A-498 human kidney epithelial cells. WAM2266 (WT), WAM5088 (*ipuS* ON/*fimS* OFF), WAM5063 (*ipuS* OFF/*fimS* OFF), WAM5064 (*ipuS* ON/*fimS* ON), and WAM5065 (*ipuS* OFF/*fimS* ON) were allowed to adhere to monolayers of A-498 cells, and then unbound bacteria were removed by washing. In a *fimS* OFF background, turning *ipuS* ON causes a 5% increase in adherence (WAM5088 versus WAM5063) ($P < 0.05$, *t* test).

kidney epithelium. Type 1 pili also promoted kidney adherence; however, locking both switches on did not cause a synergistic increase in adhesion (Fig. 7C).

DISCUSSION

Phase variation is defined as rapid and reversible ON/OFF changes in gene expression (60). It occurs by several different molecular mechanisms and contributes to virulence in multiple pathogens, including *E. coli*, *Neisseria meningitidis*, *Mycoplasma agalactiae*, *Listeria monocytogenes*, and *Clostridium difficile* (61–66), it is an advantageous form of gene regulation for pathogens as it helps a population cope with sudden changes in environmental conditions during infection (67). The presence of a subset of the population in alternative phase states circumvents the need for transcriptional and translational activation steps in response to changing conditions. CFT073 has two known phase-variable elements, *fimS* and *hyxS* (23, 45). Here, we identified a third phase-variable element (*ipuS*). We demonstrate that the orientation of the *ipuS* element in CFT073 controls the transcription of two downstream genes (*ipuR* and *upaE*), which in turn affects motility and kidney colonization in mice. Additional analysis of UpaE

revealed that it is surface localized and mediates biofilm formation and adhesion to ECM proteins.

When comparing the sequences of the half-sites, *ipuS* appears to be an intermediate between *fimS* and *hyxS* (Fig. 2). This suggests that the nonproximal recombinases FimB, FimE, and FimX would have activity at *ipuS*. Indeed, we found that FimE and FimX are catalytically active at *ipuS* (Fig. 3). Only limited sequence similarity is present between *fimS* and *hyxS* in UTI89 (45), which may account for why only the proximally encoded FimX is able to function at *hyxS* in both CFT073 and UTI89.

Though the assay described in this work was not explicitly quantitative, the five recombinases display apparent differences in their efficiency for inversion of the *ipuS* element, which indicates potential directional biases (Fig. 3). A directional bias for FimB/FimE at *fimS* has been characterized extensively in *E. coli* K-12 and is due to sequence specificity of the recombinases at the inverted repeats and surrounding sequence (22, 68–71). FimE is unable to bind to the *fimS* half-sites in the OFF orientation, which restricts its activity for catalyzing ON-to-OFF inversion. By mutating the regions outside the inverted repeats to resemble the ON or OFF state, this specificity can be reversed (69). It is possible that the apparent decreased efficiency of FimE and IpuB at *ipuS* is due to a defect in their ability to bind to the template. Electrophoretic mobility shift assays have been performed with FimB/FimE at *fimS* to characterize this effect; however, the recombinases are notoriously difficult to purify, complicating the analyses (70, 71). Further studies focused on precise assessment of catalysis and inversion frequencies, such as the application of read-mapping approaches based on deep sequencing to monitor switching (46), are needed to assess how phase bias at *ipuS* may contribute to population polarization.

The orientation of *ipuS* may also directly influence *fimS* or *hyxS* orientation, but such effects were masked by the need to lock all three switches in our analysis. Other investigators have generated *fimS*-locked strains by mutating the sequence of the inverted repeats (64). Using this approach would facilitate locking *ipuS* orientation while permitting inversion of the other two elements, helping to identify *ipuS* effects at *fimS* and *hyxS*. However, the five recombinases recognize the inverted repeats in a sequence-specific manner (69–71), so manipulating the local sequence may inherently change recombinase-binding affinity. In the context of a complete network, where multiple sites compete for limited quantities of each recombinase, changing the half-sites could perturb the orientation of the other switches by altering recombinase availability. As such, it stands to reason that the orientation of all three elements is interrelated, as they compete for a limited pool of shared enzymatic machinery.

5′ RACE analysis indicated the presence of a transcriptional start site in the *ipuS* element (Fig. 4). The promoter is part of the full-length *ipuA* coding region, and reorientation of the element turns transcription of *ipuR/upaE* ON/OFF. By sequence inspection for conserved promoter motifs proximal to the transcription start site, we were able to identify a putative *rpoD*-dependent promoter. Direct *in vitro* transcription assays using RNA polymerase holoenzyme are planned for the future to support this supposition.

ipuR is a predicted LuxR-type transcriptional regulator. LuxR-type regulators are two-domain proteins that contain an autoinducer and DNA binding domain. They have been implicated in virulence of multiple pathogens, including *Vibrio* spp., several classes of pathogenic *E. coli*, and *Mycobacterium tuberculosis*, where they often regulate systems involved in biofilm formation and motility (45, 55, 56, 72). The regulon sizes of these proteins are highly variable. Some regulate one or a few specific targets, while others have much broader effects (55). The effects of *ipuS* described here in murine infection models, tissue culture, and *in vitro* systems appear UpaE dependent. It remains unclear what role IpuR plays, if any, in the regulation of *upaE* or other target genes. While we did not observe *ipuR* dependency in the phenotypes described here, we also cannot rule out a contribution to these or other putative phenotypes. Definition of the *ipuR* regulon and its contribution to UPEC biology and pathogenesis are active areas of research.

Autotransporters are large multidomain proteins that belong to the type V secretion system (73). They possess an N-terminal signal sequence that targets the protein to the Sec machinery for transport into the periplasm, a passenger domain that is either secreted or cell surface associated, and a C-terminal translocator domain that is embedded in the outer membrane and helps facilitate translocation of the passenger domain (74–76). CFT073 possesses genes encoding multiple different autotransporters, which function as either adhesins or secreted toxins (20, 21, 51, 57, 77, 78). One well-studied autotransporter is Ag43, a surface-bound protein which is found in most *E. coli* strains, is phase variable, and mediates cell-cell adhesion, biofilm formation, and long-term colonization of the mouse bladder (49, 77, 79). Ag43 phase variation is mediated by the combined action of DAM methylase (activation) and OxyR (repression) (80–82). Additionally, altered methylation patterns in key regions modulate Ag43 transcription, and expression of Ag43 is important for facilitating infection in the murine model (77). Here, we characterize a previously uncharacterized autotransporter, UpaE, which represents another phase-variable autotransporter of *E. coli*. We show that UpaE is surface exposed and mediates biofilm formation and adherence to human ECM proteins. Our data also imply that UpaE enhances UPEC virulence based on analysis of an *ipuS* locked-ON strain in mice. Importantly, we previously observed that the *ipuA-upaE* region is more prevalent in UPEC (37%) than commensal strains (7%), suggesting this system to be a relevant virulence mechanism for many UPEC strains (23). Further studies confirming the adhesive properties of UpaE and the conditions/factors that select for its expression are in progress.

To assess the role of *ipuS* in virulence in the murine model of UTI, we infected female mice transurethrally in the bladder. We assessed colonization of the bladder and kidneys in a mixed competitive infection assay using *ipuS* locked-ON and -OFF strains, and in a type 1 fimbria locked-ON background (Fig. 7B). Locking type 1 fimbriae ON helps facilitate consistent infections as locked-OFF strains are severely attenuated (15). However, locked-ON strains have impaired swimming motility, which is also important for colonization, and type 1 fimbria expression inhibits the production of other adhesive pili, including the kidney-specific P pili (41, 83). The interrelated nature of these systems makes it difficult to study their effects in isolation and may also account for the high degree of variability observed in animal models. Further development of phase-locked *ipuS* strains that are decoupled from *fimS* and *hyxS* inversion is under way to evaluate *ipuS*-specific effects.

Tyrosine recombinases often function at invertible elements encoded in close proximity to themselves (44). However, there are exceptions to this generalization. For example, in-depth analysis of *Bacteroides fragilis* has revealed extensive networks of switches and recombinases that function at local and distant sites in the chromosome (84–88). One such enzyme, Mpi, can catalyze inversion of 13 elements located throughout the *B. fragilis* chromosome (88). This inversion network controls the expression of surface architecture components and is predicted to function as a mechanism for global surface remodeling in response to changing environmental conditions (85, 88). The identification of *ipuS* demonstrated recombinase cross-reactivity among the three invertible elements, and known environmental stimuli that influence inversion of the switches (38, 39, 89, 90) suggest the existence of a complex network in UPEC (23, 45). UPEC encounters a variety of different conditions during colonization of a human host, for example, in the gut, urethra, bladder, kidneys, and bloodstream. We hypothesize that population heterogeneity generated by multiple mechanisms, including differential gene regulation, epigenetic regulation, and the phase-variable network described here, provides a means for UPEC to successfully colonize these different environments.

MATERIALS AND METHODS

Bacterial strains, cell lines, plasmids, and culture conditions. All of the strains, cell lines, and plasmids used in this study are listed in Table 1. In-frame deletion mutants of CFT073 were generated using a modification of the Lambda Red method of homologous recombination to include phage transduction of the marker into a clean genetic background by ϕEB49 prior to removal of the cassette via pCP20 (91, 92). Phase-locked mutants were generated by sequential deletion of the five previously

described tyrosine recombinases in CFT073 (23). Upon deletion of the final recombinase, multiple colonies were screened to identify mutants with all four possible combinations of *fimS* and *ipuS* phase states. *lacZ* transcriptional fusions were generated using methods described previously with the suicide vector pFUSE (93). All strains were cultivated in Luria-Bertani (LB) broth or LB agar or on MacConkey lactose medium unless otherwise indicated. Antibiotic selection employing kanamycin (50 μg/ml), chloramphenicol (20 μg/ml), or carbenicillin (250 μg/ml) was used as appropriate.

The kidney epithelial cell line A-498 (ATCC HTB-44) was grown in RPMI 1640 with L-glutamine (Mediatech, Inc.) supplemented with 20% fetal bovine serum (Atlanta Biologicals, Lawrenceville, GA), 10 mM HEPES, and 1 mM sodium pyruvate (Mediatech, Inc.). Cells were grown at 37°C with 5% CO_2 and utilized at less than 10 passages.

***ipuS* switch state analysis.** The *ipuS* region was amplified by PCR using GoTaq Green master mix (Promega) from 0.5 μl of overnight LB broth cultures using the forward primer 5′ GTGGCGATGGGAAG GAAACG 3′ and reverse primer 5′ AAAACCCCGCCAACGCATACTC 3′. Thermocycling conditions were 94°C for 2 min; 25 cycles of 94°C for 30 s, 57°C for 30 s, and 72°C for 1 min 30 s; and 72°C for 7 min. The resulting 1,289-bp product was purified using a QIAquick PCR purification kit (Qiagen) and digested with PacI (New England BioLabs). Digested fragments were electrophoresed through a 2% agarose gel and stained with ethidium bromide. Sizes of the restriction products correspond to the state of the switch (407 bp and 882 bp, phase ON; 186 bp and 1,103 bp, phase OFF).

Construction of plasmids. The *fimB*, *fimE*, *fimX*, *ipuA*, and *ipuB* CFT073 recombinases were cloned into either pACYC177 or pACYC184. For constructs built within the pACYC177 backbone, the respective recombinase genes were constitutively expressed from the plasmid-carried kanamycin resistance gene promoter. For constructs built within the pACYC184 backbone, the respective recombinase genes were expressed from their native promoter. The *upaE* gene was amplified from CFT073 with primers 7799 (5′ GACCTGCAGGCATGCAAGCTATGAAGGAGGAGTGGTATGAATAAAGTATATAAAG 3′) and 7800 (5′ CGA CGGCCAGTGCCAAGCTTTAGAATATATATTTAATACC 3′) and inserted into pSU2718 using a modified ligation-independent cloning protocol (94). Briefly, the pSU2718 plasmid was digested with HindIII, and both cut plasmid and PCR product were treated with T4 polymerase to generate complementary overhangs. The T4 polymerase-treated insert and plasmid were mixed in a 3:1 ratio and incubated on ice for 30 min to generate pUpaE. All plasmids were confirmed by PCR and sequencing of the inserts.

5′ RACE of *ipuS* element. The *ipuS* transcription start site was identified using 5′ rapid amplification of cDNA ends (5′ RACE) (Invitrogen). Gene-specific nested primers were designed according to the manufacturer's instructions. RNA was extracted from 1 ml of a log-phase (optical density at 600 nm [OD_{600}] of 0.5) culture of WAM5064 and WAM5065 using Trizol reagent (Invitrogen). Contaminating DNA was removed by on-column DNase treatment and Pure Link RNA spin column purification (Invitrogen, Grand Island, NY), and the resulting purified RNA samples were stored in nuclease-free water at −20°C. Aliquots of the isolated RNA were processed using the 5′ RACE kit and gene-specific primers (Invitrogen) according to the manufacturer's instructions. The resulting PCR products were sequenced using Sanger dideoxy chain termination sequencing to identify putative transcription start sites.

UpaE polyclonal antibody production and Western blotting. Rabbit polyclonal anti-UpaE serum was raised to a recombinant maltose binding protein *malE-upaE* gene fusion using the pMal-p2x vector (New England BioLabs). Residues S24 to G2000 of UpaE were present in the fusion protein. Expression of the fusion protein was induced by addition of isopropyl-β-D-thiogalactopyranoside (IPTG) to the growth medium. Inclusion bodies containing the large fusion protein were solubilized in crack buffer (2% sodium dodecyl sulfate [SDS], 10% glycerol, 5% β-mercaptoethanol, 1 mM bromophenol blue, 62 mM Tris) subjected to SDS-polyacrylamide gel electrophoresis (SDS-PAGE). The large Coomassie blue-stained fusion protein band was excised from the gels and then used as an immunogen in rabbits.

In vivo expression of UpaE was determined by Western blotting. Cell pellets were solubilized in crack buffer and subjected to SDS-PAGE in 10% polyacrylamide gels. Concentrated culture supernatants were prepared by taking 10 ml of filtered late-log-phase L-broth and adding trichloroacetic acid to make a final 10% concentration. After overnight incubation at 0 to 4°F, precipitates were collected by centrifugation and solubilized in 20 μl of crack buffer. Tris at 1 M in 1-μl volumes was added until the resuspended pellet changed from yellow to blue. Protein detection was performed using the primary UpaE polyclonal antibody described above, secondary anti-rabbit-horseradish peroxidase (HRP) (Bio-Rad), and chemiluminescent detection by Amersham ECL Prime Western blotting kit (GE Healthcare).

Immunofluorescence microscopy. Immunofluorescence microscopy was performed essentially as previously described (53). Overnight cultures supplemented with the appropriate antibiotics and 1 mM IPTG were fixed to an OD_{600} of 0.4, spotted onto a glass slide, and allowed to dry. The cells were fixed with 4% paraformaldehyde (PFA), washed with phosphate-buffered saline (PBS), and blocked with 0.5% bovine serum albumin (BSA). The slides were incubated with the anti-UpaE antibody, washed with PBS, and further incubated with a secondary goat anti-rabbit antiserum coupled to fluorescein isothiocyanate (FITC). The slides were washed, air dried, mounted with ProLong Gold (Invitrogen), and examined under a Zeiss Axioplan 2 epifluorescence microscope.

Biofilm assay. Polyvinyl chloride (PVC) 96-well microtiter plates (Corning) were used to monitor biofilm formation as previously described (95). Briefly, cells were grown for 18 h in LB at 37°C, washed to remove unbound cells, and stained with 0.1% crystal violet. Quantification of the cells was performed by dissolving the crystal violet with ethanol-acetone (80:20) and taking the absorbance reads at OD_{595}. Results were presented as the mean from eight replicate wells from three independent experiments. The data were analyzed using the unpaired Student *t* test with GraphPad Prism 7 software. The graph represents results of three independent experiments with standard deviations included.

ECM adhesion assay. Bacterial binding to ECM proteins was performed in a microtiter plate enzyme-linked immunosorbent assay (51). Briefly, microtiter plates (MaxiSorp; Nunc) were coated overnight with MaxGel human ECM (10 μg/ml) or 2 μg/ml of collagen (types I to V), fibronectin, fibrinogen, laminin, or bovine serum albumin (BSA) (Sigma-Aldrich). Wells were washed with TBS (137 mM NaCl, 10 mM Tris, pH 7.4) and blocked with TBS-2% milk for 1 h. Bacterial cultures were standardized to an OD_{600} of 0.1 in TBS, and 200 μl of the cultures was added to the plates. After washing to remove unbound cells, adherent bacteria were fixed with 4% PFA, washed, and incubated with an anti-*E. coli* serum (Meridian Life Sciences, Inc.) for 1 h. The cells were washed and incubated with a secondary anti-rabbit horseradish peroxidase-conjugated antibody for another 1 h. Following a final wash, adherent bacteria were detected by adding 50 μl of tetramethylbenzidine (TMB). After 15 min, 50 μl of 1 M HCl was added to stop the reaction, and the absorbance was read at OD_{450}. The data were analyzed using the unpaired Student *t* test with GraphPad Prism 7 software. The graph represents results of three independent experiments with standard deviations included.

Swimming motility assay. Strains were grown in LB broth with appropriate selection overnight at 37°C with shaking. The overnight cultures were normalized to an OD_{600} of 0.5, and 1 μl was inoculated directly into the center of a petri plate containing 20 ml of Adler's motility medium (0.3% agar, 0.5% NaCl, 1.0% tryptone) ($n = 7$). Plates were incubated lid side up at room temperature for approximately 21 h. The diameter of the zone of swimming was measured twice at perpendicular angles for each plate, and the averages were plotted. The data were analyzed using the data analysis software package Prism (GraphPad) to determine statistically significant differences ($P < 0.05$) between strains by the Mann-Whitney test.

Kidney epithelial cell adherence assay. A-498 cells were seeded into 12-well plates at 2.5×10^5 cells/well and grown to near confluence. Monolayers were washed two times with assay medium (serum- and antibiotic-free culture medium) and preincubated for 20 min at 4°C in 1 ml assay medium. Triplicate wells were inoculated with bacteria (MOI of 10) and were settled onto host cells by centrifugation at 500 $\times$ *g* for 5 min. After 1 h of incubation at 4°C, monolayers were washed three times with Hanks balanced salt solution (HBSS) (HyClone), incubated for 5 min at 37°C in 500 μl 0.025% trypsin-0.03% EDTA in HBSS, lysed with 0.1% Triton X-100 in double-distilled water (ddH_2O), and plated on LB agar plates. Adherence was calculated as the ratio of the number of bacteria recovered to the number of bacteria inoculated into each well and expressed as percent adherence. The data were analyzed using the data analysis software package Prism (GraphPad) to determine statistically significant differences between strains by the unpaired Student *t* test.

Murine model of UTI. Six-week-old female CBA/J (Harlan Laboratories) mice were used for all infections. Cells were grown in static LB broth, and infections were performed as described previously (59, 96). For competitive infections, WAM5146, a *lacZYA* mutant variant of WAM5065, was used to facilitate generation of competitive indexes with MacConkey's lactose medium. Previous experiments indicate that *lacZYA* activity has no influence on colonization in the murine model of UTI (97). When using locked strains to examine the effects of *ipuS* variable-phase states in the mouse, the type 1 fimbria locked-ON versions were used in order to facilitate consistent infections as type 1-deficient UPEC strains are severely attenuated (15). Bars in presented data indicate the medians of the non-Gaussian-distributed data sets. Wilcoxon signed-rank tests were performed with Prism (GraphPad Software, Inc., La Jolla, CA) to determine statistical significance, and significance was reported when *P* was <0.05. This study was done in strict agreement with the recommendations found in reference 98. The murine model UTI protocol was approved by the UW—Madison Animal Care and Use Committee (permit no. M00450-0-07-08).

SUPPLEMENTAL MATERIAL

Supplemental material for this article may be found at https://doi.org/10.1128/mBio.01360-18.

FIG S1, PDF file, 0.03 MB.

ACKNOWLEDGMENTS

This work was supported by National Institutes of Health (NIH) grant R01-DK063250-07, grants from the National Health and Medical Research Council (NHMRC) of Australia, a Robert Turell Professorship awarded to R. A. Welch, and an NHMRC Senior Research Fellowship awarded to M. A. Schembri.

REFERENCES

1. Foxman B. 2014. Urinary tract infection syndromes: occurrence, recurrence, bacteriology, risk factors, and disease burden. Infect Dis Clin North Am 28:1–13. https://doi.org/10.1016/j.idc.2013.1009.1003.
2. Kunin CM. 1994. Urinary tract infections in females. Clin Infect Dis 18:1–10.
3. Haley RW, Culver DH, White JW, Morgan WM, Emori TG, Munn VP, Hooton TM. 1985. The efficacy of infection surveillance and control programs in preventing nosocomial infections in US hospitals. Am J Epidemiol 121:182–205. https://doi.org/10.1093/oxfordjournals.aje.a113990.
4. Aronson M, Medalia O, Amichay D, Nativ O. 1988. Endotoxin-induced shedding of viable uroepithelial cells is an antimicrobial defense mechanism. Infect Immun 56:1615–1617.
5. Wu XR, Kong XP, Pellicer A, Kreibich G, Sun TT. 2009. Uroplakins in urothelial biology, function, and disease. Kidney Int 75:1153–1165. https://doi.org/10.1038/ki.2009.73.
6. Nielubowicz GR, Mobley HL. 2010. Host-pathogen interactions in urinary tract infection. Nat Rev Urol 7:430–441. https://doi.org/10.1038/nrurol.2010.101.
7. Sivick KE, Mobley HL. 2010. Waging war against uropathogenic Esche-

richia coli: winning back the urinary tract. Infect Immun 78:568–585. https://doi.org/10.1128/IAI.01000-09.
8. Haraoka M, Hang L, Frendéus B, Godaly G, Burdick M, Strieter R, Svanborg C. 1999. Neutrophil recruitment and resistance to urinary tract infection. J Infect Dis 180:1220–1229. https://doi.org/10.1086/315006.
9. Lundberg JO, Ehrén I, Jansson O, Adolfsson J, Lundberg JM, Weitzberg E, Alving K, Wiklund NP. 1996. Elevated nitric oxide in the urinary bladder in infectious and noninfectious cystitis. Urology 48:700–702. https://doi.org/10.1016/S0090-4295(96)00423-2.
10. Shahin RD, Engberg I, Hagberg L, Svanborg Edén C. 1987. Neutrophil recruitment and bacterial clearance correlated with LPS responsiveness in local gram-negative infection. J Immunol 138:3475–3480.
11. Hannan TJ, Totsika M, Mansfield KJ, Moore KH, Schembri MA, Hultgren SJ. 2012. Host-pathogen checkpoints and population bottlenecks in persistent and intracellular uropathogenic Escherichia coli bladder infection. FEMS Microbiol Rev 36:616–648. https://doi.org/10.1111/j.1574-6976.2012.00339.x.
12. Gilbert NM, O'Brien VP, Lewis AL. 2017. Transient microbiota exposures activate dormant Escherichia coli infection in the bladder and drive severe outcomes of recurrent disease. PLoS Pathog 13:e1006238. https://doi.org/10.1371/journal.ppat.1006238.
13. Gottschick C, Deng ZL, Vital M, Masur C, Abels C, Pieper DH, Wagner-Döbler I. 2017. The urinary microbiota of men and women and its changes in women during bacterial vaginosis and antibiotic treatment. Microbiome 5:99. https://doi.org/10.1186/s40168-017-0305-3.
14. Bahrani-Mougeot FK, Buckles EL, Lockatell CV, Hebel JR, Johnson DE, Tang CM, Donnenberg MS. 2002. Type 1 fimbriae and extracellular polysaccharides are preeminent uropathogenic Escherichia coli virulence determinants in the murine urinary tract. Mol Microbiol 45:1079–1093. https://doi.org/10.1046/j.1365-2958.2002.03078.x.
15. Connell I, Agace W, Klemm P, Schembri M, Mărild S, Svanborg C. 1996. Type 1 fimbrial expression enhances Escherichia coli virulence for the urinary tract. Proc Natl Acad Sci U S A 93:9827–9832. https://doi.org/10.1073/pnas.93.18.9827.
16. Guyer DM, Radulovic S, Jones FE, Mobley HL. 2002. Sat, the secreted autotransporter toxin of uropathogenic Escherichia coli, is a vacuolating cytotoxin for bladder and kidney epithelial cells. Infect Immun 70:4539–4546. https://doi.org/10.1128/IAI.70.8.4539-4546.2002.
17. Keith BR, Maurer L, Spears PA, Orndorff PE. 1986. Receptor-binding function of type 1 pili effects bladder colonization by a clinical isolate of Escherichia coli. Infect Immun 53:693–696.
18. Mobley HL, Green DM, Trifillis AL, Johnson DE, Chippendale GR, Lockatell CV, Jones BD, Warren JW. 1990. Pyelonephritogenic Escherichia coli and killing of cultured human renal proximal tubular epithelial cells: role of hemolysin in some strains. Infect Immun 58:1281–1289.
19. Torres AG, Redford P, Welch RA, Payne SM. 2001. TonB-dependent systems of uropathogenic Escherichia coli: aerobactin and heme transport and TonB are required for virulence in the mouse. Infect Immun 69:6179–6185. https://doi.org/10.1128/IAI.69.10.6179-6185.2001.
20. Allsopp LP, Beloin C, Ulett GC, Valle J, Totsika M, Sherlock O, Ghigo JM, Schembri MA. 2012. Molecular characterization of UpaB and UpaC, two new autotransporter proteins of uropathogenic Escherichia coli CFT073. Infect Immun 80:321–332. https://doi.org/10.1128/IAI.05322-11.
21. Heimer SR, Rasko DA, Lockatell CV, Johnson DE, Mobley HL. 2004. Autotransporter genes pic and tsh are associated with Escherichia coli strains that cause acute pyelonephritis and are expressed during urinary tract infection. Infect Immun 72:593–597. https://doi.org/10.1128/IAI.72.1.593-597.2004.
22. Leathart JB, Gally DL. 1998. Regulation of type 1 fimbrial expression in uropathogenic Escherichia coli: heterogeneity of expression through sequence changes in the fim switch region. Mol Microbiol 28:371–381. https://doi.org/10.1046/j.1365-2958.1998.00802.x.
23. Bryan A, Roesch P, Davis L, Moritz R, Pellett S, Welch RA. 2006. Regulation of type 1 fimbriae by unlinked FimB- and FimE-like recombinases in uropathogenic Escherichia coli strain CFT073. Infect Immun 74:1072–1083. https://doi.org/10.1128/IAI.74.2.1072-1083.2006.
24. Cooper LA, Simmons LA, Mobley HL. 2012. Involvement of mismatch repair in the reciprocal control of motility and adherence of uropathogenic Escherichia coli. Infect Immun 80:1969–1979. https://doi.org/10.1128/IAI.00043-12.
25. Spaulding CN, Klein RD, Ruer S, Kau AL, Schreiber HL, Cusumano ZT, Dodson KW, Pinkner JS, Fremont DH, Janetka JW, Remaut H, Gordon JI, Hultgren SJ. 2017. Selective depletion of uropathogenic E. coli from the gut by a FimH antagonist. Nature 546:528–532. https://doi.org/10.1038/nature22972.
26. Eisenstein BI. 1981. Phase variation of type 1 fimbriae in Escherichia coli is under transcriptional control. Science 214:337–339. https://doi.org/10.1126/science.6116279.
27. Abraham JM, Freitag CS, Clements JR, Eisenstein BI. 1985. An invertible element of DNA controls phase variation of type 1 fimbriae of Escherichia coli. Proc Natl Acad Sci U S A 82:5724–5727. https://doi.org/10.1073/pnas.82.17.5724.
28. Klemm P. 1986. Two regulatory fim genes, fimB and fimE, control the phase variation of type 1 fimbriae in Escherichia coli. EMBO J 5:1389–1393.
29. Chen Y, Narendra U, Iype LE, Cox MM, Rice PA. 2000. Crystal structure of a Flp recombinase-Holliday junction complex: assembly of an active oligomer by helix swapping. Mol Cell 6:885–897. https://doi.org/10.1016/S1097-2765(00)00086-1.
30. Corcoran CP, Dorman CJ. 2009. DNA relaxation-dependent phase biasing of the fim genetic switch in Escherichia coli depends on the interplay of H-NS, IHF and LRP. Mol Microbiol 74:1071–1082. https://doi.org/10.1111/j.1365-2958.2009.06919.x.
31. Gopaul DN, Duyne GD. 1999. Structure and mechanism in site-specific recombination. Curr Opin Struct Biol 9:14–20. https://doi.org/10.1016/S0959-440X(99)80003-7.
32. Grindley ND, Whiteson KL, Rice PA. 2006. Mechanisms of site-specific recombination. Annu Rev Biochem 75:567–605. https://doi.org/10.1146/annurev.biochem.73.011303.073908.
33. Kelly A, Conway C, O Cróinín T, Smith SG, Dorman CJ. 2006. DNA supercoiling and the Lrp protein determine the directionality of fim switch DNA inversion in Escherichia coli K-12. J Bacteriol 188:5356–5363. https://doi.org/10.1128/JB.00344-06.
34. Dorman CJ, Higgins CF. 1987. Fimbrial phase variation in Escherichia coli: dependence on integration host factor and homologies with other site-specific recombinases. J Bacteriol 169:3840–3843. https://doi.org/10.1128/jb.169.8.3840-3843.1987.
35. Blomfield IC, Calie PJ, Eberhardt KJ, McClain MS, Eisenstein BI. 1993. Lrp stimulates phase variation of type 1 fimbriation in Escherichia coli K-12. J Bacteriol 175:27–36. https://doi.org/10.1128/jb.175.1.27-36.1993.
36. O'Gara JP, Dorman CJ. 2000. Effects of local transcription and H-NS on inversion of the fim switch of Escherichia coli. Mol Microbiol 36:457–466. https://doi.org/10.1046/j.1365-2958.2000.01864.x.
37. Roesch PL, Blomfield IC. 1998. Leucine alters the interaction of the leucine-responsive regulatory protein (Lrp) with the fim switch to stimulate site-specific recombination in Escherichia coli. Mol Microbiol 27:751–761. https://doi.org/10.1046/j.1365-2958.1998.00720.x.
38. Schwan WR, Lee JL, Lenard FA, Matthews BT, Beck MT. 2002. Osmolarity and pH growth conditions regulate fim gene transcription and type 1 pilus expression in uropathogenic Escherichia coli. Infect Immun 70:1391–1402. https://doi.org/10.1128/IAI.70.3.1391-1402.2002.
39. Kuwahara H, Myers CJ, Samoilov MS. 2010. Temperature control of fimbriation circuit switch in uropathogenic Escherichia coli: quantitative analysis via automated model abstraction. PLoS Comput Biol 6:e1000723. https://doi.org/10.1371/journal.pcbi.1000723.
40. Müller CM, Aberg A, Straseviçiene J, Emody L, Uhlin BE, Balsalobre C. 2009. Type 1 fimbriae, a colonization factor of uropathogenic Escherichia coli, are controlled by the metabolic sensor CRP-cAMP. PLoS Pathog 5:e1000303. https://doi.org/10.1371/journal.ppat.1000303.
41. Snyder JA, Haugen BJ, Lockatell CV, Maroncle N, Hagan EC, Johnson DE, Welch RA, Mobley HL. 2005. Coordinate expression of fimbriae in uropathogenic Escherichia coli. Infect Immun 73:7588–7596. https://doi.org/10.1128/IAI.73.11.7588-7596.2005.
42. Holden NJ, Totsika M, Mahler E, Roe AJ, Catherwood K, Lindner K, Dobrindt U, Gally DL. 2006. Demonstration of regulatory cross-talk between P fimbriae and type 1 fimbriae in uropathogenic Escherichia coli. Microbiology 152:1143–1153. https://doi.org/10.1099/mic.0.28677-0.
43. Lindberg S, Xia Y, Sondén B, Göransson M, Hacker J, Uhlin BE. 2008. Regulatory Interactions among adhesin gene systems of uropathogenic Escherichia coli. Infect Immun 76:771–780. https://doi.org/10.1128/IAI.01010-07.
44. Johnson RC. 2002. Bacterial site-specific DNA inversion systems, p 230–271. *In* Craig NL, Craigie R, Gellert M, Lambowitz AM (ed), Mobile DNA II. ASM Press, Washington, DC.
45. Bateman SL, Seed PC. 2012. Epigenetic regulation of the nitrosative stress response and intracellular macrophage survival by extraintestinal pathogenic Escherichia coli. Mol Microbiol 83:908–925. https://doi.org/10.1111/j.1365-2958.2012.07977.x.

46. Sarkar S, Roberts LW, Phan MD, Tan L, Lo AW, Peters KM, Paterson DL, Upton M, Ulett GC, Beatson SA, Totsika M, Schembri MA. 2016. Comprehensive analysis of type 1 fimbriae regulation in fimB-null strains from the multidrug resistant Escherichia coli ST131 clone. Mol Microbiol 101:1069–1087. https://doi.org/10.1111/mmi.13442.
47. Reznikoff WS, Siegele DA, Cowing DW, Gross CA. 1985. The regulation of transcription initiation in bacteria. Annu Rev Genet 19:355–387. https://doi.org/10.1146/annurev.ge.19.120185.002035.
48. Allsopp LP, Totsika M, Tree JJ, Ulett GC, Mabbett AN, Wells TJ, Kobe B, Beatson SA, Schembri MA. 2010. UpaH is a newly identified autotransporter protein that contributes to biofilm formation and bladder colonization by uropathogenic Escherichia coli CFT073. Infect Immun 78:1659–1669. https://doi.org/10.1128/IAI.01010-09.
49. Heras B, Totsika M, Peters KM, Paxman JJ, Gee CL, Jarrott RJ, Perugini MA, Whitten AE, Schembri MA. 2014. The antigen 43 structure reveals a molecular Velcro-like mechanism of autotransporter-mediated bacterial clumping. Proc Natl Acad Sci U S A 111:457–462. https://doi.org/10.1073/pnas.1311592111.
50. Wells TJ, Sherlock O, Rivas L, Mahajan A, Beatson SA, Torpdahl M, Webb RI, Allsopp LP, Gobius KS, Gally DL, Schembri MA. 2008. EhaA is a novel autotransporter protein of enterohemorrhagic Escherichia coli O157:H7 that contributes to adhesion and biofilm formation. Environ Microbiol 10:589–604. https://doi.org/10.1111/j.1462-2920.2007.01479.x.
51. Valle J, Mabbett AN, Ulett GC, Toledo-Arana A, Wecker K, Totsika M, Schembri MA, Ghigo JM, Beloin C. 2008. UpaG, a new member of the trimeric autotransporter family of adhesins in uropathogenic Escherichia coli. J Bacteriol 190:4147–4161. https://doi.org/10.1128/JB.00122-08.
52. Wells TJ, McNeilly TN, Totsika M, Mahajan A, Gally DL, Schembri MA. 2009. The Escherichia coli O157:H7 EhaB autotransporter protein binds to laminin and collagen I and induces a serum IgA response in O157:H7 challenged cattle. Environ Microbiol 11:1803–1814. https://doi.org/10.1111/j.1462-2920.2009.01905.x.
53. Martinez-Gil M, Goh KGK, Rackaityte E, Sakamoto C, Audrain B, Moriel DG, Totsika M, Ghigo JM, Schembri MA, Beloin C. 2017. YeeJ is an inverse autotransporter from Escherichia coli that binds to peptidoglycan and promotes biofilm formation. Sci Rep 7:11326. https://doi.org/10.1038/s41598-017-10902-0.
54. Kanamaru K, Kanamaru K, Tatsuno I, Tobe T, Sasakawa C. 2000. SdiA, an Escherichia coli homologue of quorum-sensing regulators, controls the expression of virulence factors in enterohaemorrhagic Escherichia coli O157:H7. Mol Microbiol 38:805–816. https://doi.org/10.1046/j.1365-2958.2000.02171.x.
55. Chen J, Xie J. 2011. Role and regulation of bacterial LuxR-like regulators. J Cell Biochem 112:2694–2702. https://doi.org/10.1002/jcb.23219.
56. Martínez-Santos VI, Medrano-López A, Saldaña Z, Girón JA, Puente JL. 2012. Transcriptional regulation of the ecp operon by EcpR, IHF, and H-NS in attaching and effacing Escherichia coli. J Bacteriol 194:5020–5033. https://doi.org/10.1128/JB.00915-12.
57. Parham NJ, Srinivasan U, Desvaux M, Foxman B, Marrs CF, Henderson IR. 2004. PicU, a second serine protease autotransporter of uropathogenic Escherichia coli. FEMS Microbiol Lett 230:73–83. https://doi.org/10.1016/S0378-1097(03)00862-0.
58. Navarro-Garcia F, Gutierrez-Jimenez J, Garcia-Tovar C, Castro LA, Salazar-Gonzalez H, Cordova V. 2010. Pic, an autotransporter protein secreted by different pathogens in the Enterobacteriaceae family, is a potent mucus secretagogue. Infect Immun 78:4101–4109. https://doi.org/10.1128/IAI.00523-10.
59. Hryckowian AJ, Welch RA. 2013. RpoS contributes to phagocyte oxidase-mediated stress resistance during urinary tract infection by Escherichia coli CFT073. mBio 4:e00023-13. https://doi.org/10.1128/mBio.00023-13.
60. Henderson IR, Owen P, Nataro JP. 1999. Molecular switches—the ON and OFF of bacterial phase variation. Mol Microbiol 33:919–932. https://doi.org/10.1046/j.1365-2958.1999.01555.x.
61. Chopra-Dewasthaly R, Citti C, Glew MD, Zimmermann M, Rosengarten R, Jechlinger W. 2008. Phase-locked mutants of Mycoplasma agalactiae: defining the molecular switch of high-frequency Vpma antigenic variation. Mol Microbiol 67:1196–1210. https://doi.org/10.1111/j.1365-2958.2007.06103.x.
62. Lindbäck T, Secic I, Rørvik LM. 2011. A contingency locus in prfA in a Listeria monocytogenes subgroup allows reactivation of the PrfA virulence regulator during infection in mice. Appl Environ Microbiol 77:3478–3483. https://doi.org/10.1128/AEM.02708-10.
63. Srikhanta YN, Dowideit SJ, Edwards JL, Falsetta ML, Wu HJ, Harrison OB, Fox KL, Seib KL, Maguire TL, Wang AH, Maiden MC, Grimmond SM, Apicella MA, Jennings MP. 2009. Phasevarions mediate random switching of gene expression in pathogenic Neisseria. PLoS Pathog 5:e1000400. https://doi.org/10.1371/journal.ppat.1000400.
64. Gunther NW, IV, Snyder JA, Lockatell V, Blomfield I, Johnson DE, Mobley HL. 2002. Assessment of virulence of uropathogenic Escherichia coli type 1 fimbrial mutants in which the invertible element is phase-locked on or off. Infect Immun 70:3344–3354. https://doi.org/10.1128/IAI.70.7.3344-3354.2002.
65. Anjuwon-Foster BR, Tamayo R. 2017. A genetic switch controls the production of flagella and toxins in Clostridium difficile. PLoS Genet 13:e1006701. https://doi.org/10.1371/journal.pgen.1006701.
66. Anjuwon-Foster BR, Tamayo R. 2018. Phase variation of Clostridium difficile virulence factors. Gut Microbes 9:76–83. https://doi.org/10.1080/19490976.2017.1362526.
67. Visco P, Allen RJ, Majumdar SN, Evans MR. 2010. Switching and growth for microbial populations in catastrophic responsive environments. Biophys J 98:1099–1108. https://doi.org/10.1016/j.bpj.2009.11.049.
68. Dove SL, Dorman CJ. 1996. Multicopy fimB gene expression in Escherichia coli: binding to inverted repeats in vivo, effect on fimA gene transcription and DNA inversion. Mol Microbiol 21:1161–1173. https://doi.org/10.1046/j.1365-2958.1996.681434.x.
69. Kulasekara HD, Blomfield IC. 1999. The molecular basis for the specificity of fimE in the phase variation of type 1 fimbriae of Escherichia coli K-12. Mol Microbiol 31:1171–1181. https://doi.org/10.1046/j.1365-2958.1999.01257.x.
70. Smith SG, Dorman CJ. 1999. Functional analysis of the FimE integrase of Escherichia coli K-12: isolation of mutant derivatives with altered DNA inversion preferences. Mol Microbiol 34:965–979. https://doi.org/10.1046/j.1365-2958.1999.01657.x.
71. Burns LS, Smith SG, Dorman CJ. 2000. Interaction of the FimB integrase with the fimS invertible DNA element in *Escherichia coli in vivo* and in vitro. J Bacteriol 182:2953–2959. https://doi.org/10.1128/JB.182.10.2953-2959.2000.
72. Tatsuno I, Nagano K, Taguchi K, Rong L, Mori H, Sasakawa C. 2003. Increased adherence to Caco-2 cells caused by disruption of the yhiE and yhiF genes in enterohemorrhagic Escherichia coli O157:H7. Infect Immun 71:2598–2606. https://doi.org/10.1128/IAI.71.5.2598-2606.2003.
73. Grijpstra J, Arenas J, Rutten L, Tommassen J. 2013. Autotransporter secretion: varying on a theme. Res Microbiol 164:562–582. https://doi.org/10.1016/j.resmic.2013.03.010.
74. Henderson IR, Navarro-Garcia F, Nataro JP. 1998. The great escape: structure and function of the autotransporter proteins. Trends Microbiol 6:370–378. https://doi.org/10.1016/S0966-842X(98)01318-3.
75. Henderson IR, Navarro-Garcia F, Desvaux M, Fernandez RC, Ala'Aldeen D. 2004. Type V protein secretion pathway: the autotransporter story. Microbiol Mol Biol Rev 68:692–744. https://doi.org/10.1128/MMBR.68.4.692-744.2004.
76. Benz I, Schmidt MA. 2011. Structures and functions of autotransporter proteins in microbial pathogens. Int J Med Microbiol 301:461–468. https://doi.org/10.1016/j.ijmm.2011.03.003.
77. Ulett GC, Valle J, Beloin C, Sherlock O, Ghigo JM, Schembri MA. 2007. Functional analysis of antigen 43 in uropathogenic Escherichia coli reveals a role in long-term persistence in the urinary tract. Infect Immun 75:3233–3244. https://doi.org/10.1128/IAI.01952-06.
78. Allsopp LP, Beloin C, Moriel DG, Totsika M, Ghigo JM, Schembri MA. 2012. Functional heterogeneity of the UpaH autotransporter protein from uropathogenic Escherichia coli. J Bacteriol 194:5769–5782. https://doi.org/10.1128/JB.01264-12.
79. Ulett GC, Webb RI, Schembri MA. 2006. Antigen-43-mediated autoaggregation impairs motility in Escherichia coli. Microbiology 152:2101–2110. https://doi.org/10.1099/mic.0.28607-0.
80. Henderson IR, Owen P. 1999. The major phase-variable outer membrane protein of Escherichia coli structurally resembles the immunoglobulin A1 protease class of exported protein and is regulated by a novel mechanism involving Dam and oxyR. J Bacteriol 181:2132–2141.
81. Haagmans W, van der Woude M. 2000. Phase variation of Ag43 in Escherichia coli: Dam-dependent methylation abrogates OxyR binding and OxyR-mediated repression of transcription. Mol Microbiol 35:877–887. https://doi.org/10.1046/j.1365-2958.2000.01762.x.
82. van der Woude MW, Henderson IR. 2008. Regulation and function of Ag43 (flu). Annu Rev Microbiol 62:153–169. https://doi.org/10.1146/annurev.micro.62.081307.162938.
83. Wright KJ, Seed PC, Hultgren SJ. 2005. Uropathogenic Escherichia coli

flagella aid in efficient urinary tract colonization. Infect Immun 73:7657–7668. https://doi.org/10.1128/IAI.73.11.7657-7668.2005.
84. Nakayama-Imaohji H, Hirakawa H, Ichimura M, Wakimoto S, Kuhara S, Hayashi T, Kuwahara T. 2009. Identification of the site-specific DNA invertase responsible for the phase variation of SusC/SusD family outer membrane proteins in Bacteroides fragilis. J Bacteriol 191:6003–6011. https://doi.org/10.1128/JB.00687-09.
85. Roche-Hakansson H, Chatzidaki-Livanis M, Coyne MJ, Comstock LE. 2007. Bacteroides fragilis synthesizes a DNA invertase affecting both a local and a distant region. J Bacteriol 189:2119–2124. https://doi.org/10.1128/JB.01362-06.
86. Cerdeño-Tárraga AM, Patrick S, Crossman LC, Blakely G, Abratt V, Lennard N, Poxton I, Duerden B, Harris B, Quail MA, Barron A, Clark L, Corton C, Doggett J, Holden MT, Larke N, Line A, Lord A, Norbertczak H, Ormond D, Price C, Rabbinowitsch E, Woodward J, Barrell B, Parkhill J. 2005. Extensive DNA inversions in the B. fragilis genome control variable gene expression. Science 307:1463–1465. https://doi.org/10.1126/science.1107008.
87. Kuwahara T, Yamashita A, Hirakawa H, Nakayama H, Toh H, Okada N, Kuhara S, Hattori M, Hayashi T, Ohnishi Y. 2004. Genomic analysis of Bacteroides fragilis reveals extensive DNA inversions regulating cell surface adaptation. Proc Natl Acad Sci U S A 101:14919–14924. https://doi.org/10.1073/pnas.0404172101.
88. Coyne MJ, Weinacht KG, Krinos CM, Comstock LE. 2003. Mpi recombinase globally modulates the surface architecture of a human commensal bacterium. Proc Natl Acad Sci U S A 100:10446–10451. https://doi.org/10.1073/pnas.1832655100.
89. Gunther NW, Lockatell V, Johnson DE, Mobley HL. 2001. In vivo dynamics of type 1 fimbria regulation in uropathogenic Escherichia coli during experimental urinary tract infection. Infect Immun 69:2838–2846. https://doi.org/10.1128/IAI.69.5.2838-2846.2001.
90. Donovan GT, Norton JP, Bower JM, Mulvey MA. 2013. Adenylate cyclase and the cyclic AMP receptor protein modulate stress resistance and virulence capacity of uropathogenic Escherichia coli. Infect Immun 81:249–258. https://doi.org/10.1128/IAI.00796-12.
91. Battaglioli EJ, Baisa GA, Weeks AE, Schroll RA, Hryckowian AJ, Welch RA. 2011. Isolation of generalized transducing bacteriophages for uropathogenic strains of Escherichia coli. Appl Environ Microbiol 77:6630–6635. https://doi.org/10.1128/AEM.05307-11.
92. Datsenko KA, Wanner BL. 2000. One-step inactivation of chromosomal genes in Escherichia coli K-12 using PCR products. Proc Natl Acad Sci U S A 97:6640–6645. https://doi.org/10.1073/pnas.120163297.
93. Bäumler AJ, Tsolis RM, van der Velden AW, Stojiljkovic I, Anic S, Heffron F. 1996. Identification of a new iron regulated locus of Salmonella typhi. Gene 183:207–213. https://doi.org/10.1016/S0378-1119(96)00560-4.
94. Eschenfeldt WH, Lucy S, Millard CS, Joachimiak A, Mark ID. 2009. A family of LIC vectors for high-throughput cloning and purification of proteins. Methods Mol Biol 498:105–115. https://doi.org/10.1007/978-1-59745-196-3_7.
95. Schembri MA, Klemm P. 2001. Biofilm formation in a hydrodynamic environment by novel FimH variants and ramifications for virulence. Infect Immun 69:1322–1328. https://doi.org/10.1128/IAI.69.3.1322-1328.2001.
96. Redford P, Roesch PL, Welch RA. 2003. DegS is necessary for virulence and is among extraintestinal Escherichia coli genes induced in murine peritonitis. Infect Immun 71:3088–3096. https://doi.org/10.1128/IAI.71.6.3088-3096.2003.
97. Redford P, Welch RA. 2006. Role of sigma E-regulated genes in Escherichia coli uropathogenesis. Infect Immun 74:4030–4038. https://doi.org/10.1128/IAI.01984-05.
98. National Research Council. 2011. Guide for the care and use of laboratory animals, 8th ed. National Academies Press, Washington, DC.